Preliminary Results of the MOSES II 2015 Flight

Roy Smart, Hans Courrier, Charles C. Kankelborg
Physics Department, Montana State University, Bozeman, MT 59717
roy.smart@montana.edu

Abstract

The Multi-Order Solar Extreme Ultraviolet Spectrograph (MOSES) is a slitless spectrograph which aims to produce simultaneous spatial-spectral imaging of the solar transition region. This is accomplished through a multilayer concave diffraction grating which produces three images for the spectral orders m = 0, ±1. The multilayer coating provides a narrow passband, dominated by Ne VII (46.5 nm), which allows the three images to be compared in order to determine line broadenings and identify explosive events in the Solar Transition Region. Here, we examine the preliminary results of MOSES II, the instrument's second flight which was launched on a sounding rocket from White Sands Missile Range, NM in August 2015. We present the first images of the Sun in Ne VII since Skylab and the preliminary results of observed doppler shifts within an active region.

MOSES Instrument

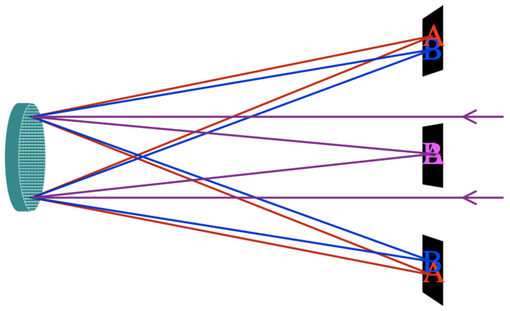

Figure 1: *Schematic of the MOSES II instrument.[1]*

MOSES II utilizes a spherical diffraction grating to form images in the +1, −1, and 0 orders. Multilayer coatings and thin film filters limit the passband of the instrument. Images formed in the non-zero orders encode spectral information along the spatial axis parallel to the dispersion plane. When viewed in the +1 and −1 image orders, a feature with a doppler shift appears translated in opposite directions along this axis. The spectral resolution of *MOSES* is 30 km/s/pixel.

Due to a combustion instability during launch, the MOSES II payload was subject to an extreme vibration environment of over 120g. This resulted in the failure of the $m = -1$ CCD and tearing of the thin film filters over the other two CCDs, severely overexposing large portions of the $m = +1$ CCD. The best data in both remaining channels is in the region outlined by the red box in Figure 2.

Furthermore, the $m = 0$ image also exhibits a bimodal PSF. We have applied a Fourier deconvolution technique to remove the double image.

Acknowledgment

This work is supported by NASA grant NNX07AG76G

Comparison with SDO Observations

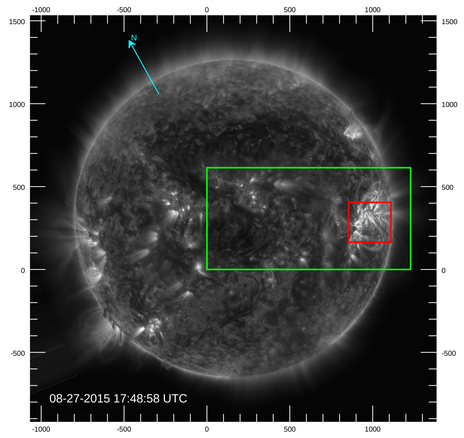

Figure 2: *AIA 171 channel visualization of MOSES II FOV and location of AR 12403.[2] Units in arcsec.*

Pictured in Figure 2 is an AIA 171 image rotated 20.8° N into the coordinate system of the *MOSES II* instrument. The FOV of *MOSES* is boxed in green.

In Figure 3, we have AR 12403 in the red region outlined in Figure 2, presented in six different ways. The top row consists of the *MOSES* $m = 0$ image (left), the $m = +1$ image (right), and the difference (center). On the bottom row we have the same region captured by the AIA 171 channel (left), the 131 channel (center), and the HMI LOS magnetogram (right). In this region we have used the difference image to select three further areas of interest outlined in green on Figure 3. We have also identified the footpoint of each event, indicated by the red circles on Figure 3.

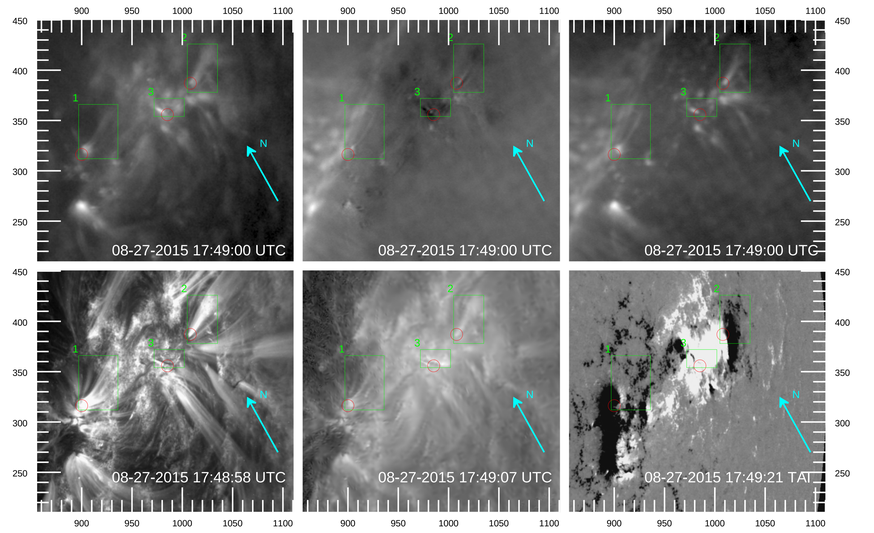

Figure 3: *AR 12403 captured by MOSES, AIA, and HMI.[2][3] Units in arcsec.*

Extracting Doppler Velocities from *MOSES II* Data

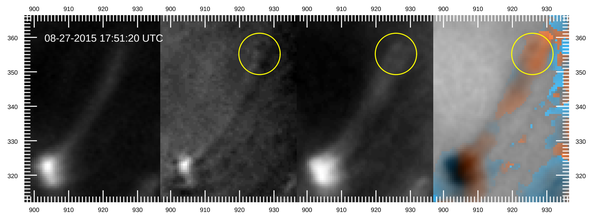

Figure 4: *Region 1, a cooling loop. Units in arcsec.*

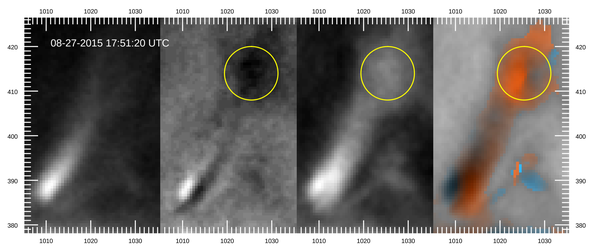

Figure 5: *Region 2, another cooling loop. Units in arcsec.*

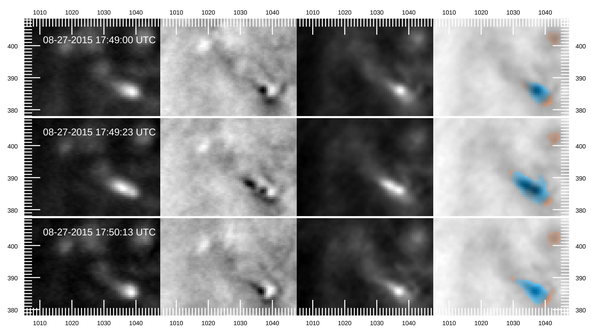

Figure 6: *Region 3, blueshifted jet. Units in arcsec.*

We use FLCT to track dispersion between the $m = 0$ and $m = +1$ order image pairs and generate dopplergrams for the MOSES II data set.[4][5] For the three features identified above, images are displayed (from left to right) of the zeroth order, difference image of the zeroth and positive order, positive order, and FLCT Dopplergram.

In Regions 1 and 2, described by Figures 4 and 5, redshifted material is observed near loop footpoints. In Region 1, the redshift ranges from 50 km/s near the center of the image to 30 km/s near the footpoint. In between the footpoint and the center of the image there is a small region that has a blue shift of −10 km/s. In Region 2 the redshift is smaller and ranges from 10 km/s at center to 25 km/s near the footpoint. This feature is redshifted along its entire path. For both of these regions LOS velocity is subsonic. Spuriously high LOS velocities (above ≈100 km/s, yellow circles in Figures 4 and 5) are likely caused by spectral contamination that exists in the $m = 0$ order but is absent in the $m = 1$ order.[6]

In Region 3, a blue-shifted jet was captured during the beginning of the exposure sequence. Figure 6 shows the evolution of this event in exposures 2, 3, and 6. The Doppler velocity averaged over the spatial extent of the event in each of these exposure is −24 km/s. The jet appears to rise and then fall back, but the blueshift persists over the lifetime of the event.

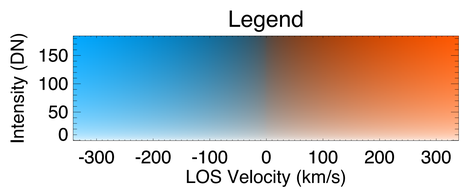

Discussion and Conclusions

In the three regions of interest shown here, measured LOS velocities are subsonic. Large LOS velocities (> 100 km/s) in these regions are the result of the inversion method finding large displacements in areas of spectral contamination and low signal.

In Regions 1 and 2, the redshifts we observe near loop footpoints may be a result of material cooling and descending along a closed loop. This provides a possible explanation for the redshift increasing near the footpoint of Feature 2, but is inconsistent with the blue shift observed near the center of the image in Region 1.

In Region 3 we observe a subsonic blue-shifted jet. Although this jet appears to rise and fall back, no redshift is observed, indicating that the accelerated material does not recede. A possible explanation for this is that the material has been heated enough that it is no longer in the MOSES II passband. This event is captured in several other AIA channels and occurs very near an area of intruding minority polarity in the HMI LOS magnetogram. Given the proximity to areas of strong magnetic field, this jet may be a result of magnetic reconnection.

References

[1] Fox, J. L., Kankelborg, C. C., & Thomas, R. J. (2010) *APJ* 719, 1132.
[2] J. R. Lemen, *et al.* (2012), *Solar Physics* doi: 10.1007/s11207-011-9776-8
[3] J. Schou, *et al.* (2012), *Solar Physics* doi: 10.1007/s11207-011-9842-2
[4] Fisher, G. H., & Welsch, B. T. (2008) *PASP* 383, 373.
[5] Courrier, H. T., & Kankelborg, C. C. (Oct. 15, 2015) *Proc. SPIE 9643* doi:10.1117/12.2194607
[6] Parker, J. Poster session P2.04 presented at: 2016 SPD Standalone Meeting; May 31-June 3; Boulder, CO